Available online at www.sciencedirect.com

SciVerse ScienceDirect

Journal of the European Ceramic Society 32 (2012) 1441–1446

www.elsevier.com/locate/jeurceramsoc

Microstructure characterization of ZrB_2–SiC composite fabricated by spark plasma sintering with $TaSi_2$ additive

Chunfeng Hu [a,b], Yoshio Sakka [a,b,c,*], Jinghui Gao [d], Hidehiko Tanaka [a], Salvatore Grasso [b,c]

[a] *World Premier International Research Center (WPI) Initiative on Materials Nanoarchitectonics (MANA), National Institute for Materials Science (NIMS), 1-2-1 Sengen, Tsukuba, Ibaraki 305-0047, Japan*

[b] *Advanced Ceramics Group, Materials Processing Unit, NIMS, 1-2-1 Sengen, Tsukuba, Ibaraki 305-0047, Japan*

[c] *Graduate School of Pure and Applied Sciences, University of Tsukuba, 1-1-1 Tennodai, Tsukuba, Ibaraki 305-8571, Japan*

[d] *Ferroic Physics Group, NIMS, 1-2-1 Sengen, Tsukuba, Ibaraki 305-0047, Japan*

Available online 17 September 2011

Abstract

Dense ZrB_2–SiC composite was synthesized by spark plasma sintering with 10 vol.% $TaSi_2$ additive. When sintered at 1600 °C, core–shell structure was found existing in the sample. The core was ZrB_2 and the shell was (Zr,Ta)B_2 solid solution. This result was ascribed to the decomposition of $TaSi_2$ and the solid solution of Ta atoms into ZrB_2 grains. The solid solution process probably decreased the boride grain boundary active energy, contributing to the formation of coherent structure of grain boundaries. Additionally, the existence of dislocations in the boride grains indicated that the applied pressure also imposed an important effect on the densification of composite. When sintered at 1800 °C, owing to the atom diffusion, Ta atoms homogeneously distributed in the boride grains, leading to the disappearance of core–shell structure. The boundaries between (Zr,Ta)B_2 grains, as well as between boride grains and SiC particles, were still clear without amorphous phase existing.

Keywords: Composite; Spark plasma sintering; Microstructure; Densification mechanism

1. Introduction

Owing to the low density (6.11 g/cm)[3], high melting point (3250 °C), high elastic modulus (491 GPa), high hardness (23 GPa), high thermal conductivity (56 W/(m K)), and high thermal shock resistance and good oxidation resistance, ZrB_2 has been considered as the potential thermal protection material for reentry space vehicles.[1–3] However, due to the strong covalent bonding in the ZrB_2 crystal structure and poor self diffusivity, it was difficult to densify it at a temperature below 2000 °C. The introduction of SiC into ZrB_2 matrix could enhance the high temperature oxidation resistance and ablation resistance of ZrB_2-based materials.[4,5] Also, the flexural strength and fracture toughness of as-formed composites were increased based on the particle-reinforcement effect.[6] However, the sintering temperature still could not be decreased largely. Recently, low melting point silicides including $ZrSi_2$ (melting point, 1620 °C), $MoSi_2$ (melting point, 2020 °C), $TaSi_2$ (melting point, 2040 °C), and Ta_5Si_3 (melting point, 2550 °C) were adopted to form the interface plastic phases, which contributed to the densification by filling up the pores in the composites during sintering. Guo et al.[7,8] determined that fully dense ZrB_2-based composites with $ZrSi_2$ could be prepared at 1550 °C under 30 MPa for 20–40 vol.% $ZrSi_2$-containing ZrB_2 powders, and ZrB_2–$MoSi_2$–SiC composites with 10–40 vol.% $MoSi_2$ could be successfully densified at 1800 °C under a pressure of 30 MPa. Sciti et al.[9] proved that dense fine grained ZrB_2-based composite containing 15 vol.% $TaSi_2$ could be produced at 1850 °C under 30 MPa. Additionally, Talmy et al.[10] investigated the system of ZrB_2–Ta_5Si_3 and found that the composite with the additive of only 8 vol.% Ta_5Si_3 resulted in nearly full densification when sintered at 1900 °C under 20 MPa. For using $TaSi_2$ additive, it was found that core–shell structure existed in the sintered samples. It was confirmed that the decomposition of $TaSi_2$ and solid solution of Ta atoms into ZrB_2 grains led to the formation of (Zr,Ta)B_2 shell. Very recently, Hu et al.[11] synthesized the dense ZrB_2–SiC composites with $TaSi_2$ additive at a low temperature of 1600 °C by spark plasma sintering and found that the

* Corresponding author at: Nano Ceramics Center, National Institute for Materials Science (NIMS), 1-2-1 Sengen, Tsukuba, Ibaraki 305-0047, Japan. Tel.: +81 29 859 2461; fax: +81 29 859 2401.

E-mail address: sakka.yoshio@nims.go.jp (Y. Sakka).

0955-2219/$ – see front matter © 2011 Elsevier Ltd. All rights reserved.
doi:10.1016/j.jeurceramsoc.2011.08.024

core–shell structure could be removed by increasing the sintering temperature up to 1800 °C. The mechanism was due to the homogeneous distribution of Ta atoms in the ZrB_2 grains based on the atom thermal diffusion. There was one interesting phenomenon that when the low content of $TaSi_2$ (10 vol.%) was used there was no $TaSi_2$ left in the sintered samples, which meant that $TaSi_2$ has completely decomposed. All of the Ta atoms have entered the ZrB_2 grains to form solid solution shell. For this case, it was not right to simply say that the plastic deformation of $TaSi_2$ imposed obvious effect on the densification of composites. Mizuguchi et al.[12] investigated the microstructure of hot-pressed ZrB_2 with $MoSi_2$ additive and determined that Mo existed in the ZrB_2 grain boundaries. They considered that the existence of Mo probably decreased the activation energy for densification process, which contributed to the diffusion process during sintering. Probably, this mechanism could also be suitable to explain present ZrB_2–SiC–$TaSi_2$ system.

In this paper, ZrB_2–SiC composite with the additive of 10 vol.% $TaSi_2$ was synthesized at 1600 °C by spark plasma sintering.[13–15] The microstructure of as-prepared sample was investigated to explain the densification mechanisms. Additionally, the composite fabricated at 1800 °C was also prepared for comparison.

2. Experimental procedures

Commercial powders of ZrB_2 (99%, 2 μm) (Rare Metallic Co., Ltd., Japan), α-SiC (99%, 0.55 μm) (Yakushima Denko Co., Ltd, Japan), and $TaSi_2$ (99%, 2–5 μm) (Japan New Metals Co., Ltd., Japan) were used to synthesize the composite. The needed composition was 80 vol.% ZrB_2 with 10 vol.% SiC and 10 vol.% $TaSi_2$. The powders were weighed by an electrical balance with the accuracy of 10^{-2} g. The weighed powders were mixed for 24 h in a SiC jar with ethanol as the dispersant. The milling media was silicon carbide balls with a diameter of 4 mm and the milling speed was 150 rpm. After milling, the slurry was dried in air and then sieved using a 125 mesh sieve. In order to densify as-obtained powder, the mixture was put into a graphite die with a diameter of 20 mm. A layer of flexile graphite paper (~0.2 mm thickness) was set into the inner wall of die for lubrication and filling the gap between punches and die, and the die was wrapped using a layer of carbon fiber for inhibiting the rapid heat diffusion. Then the mixture was cold-pressed as a compact green body and the green body together with the die was heated in a spark plasma sintering facility (100 kN SPS-1050, Syntex Inc., Japan) in vacuum (10^{-2} Pa). Each pulse lasted 3.3 ms and the duty cycle was 12 pulses on and 2 pulses off. The temperature was measured by an optical pyrometer focusing on a hole in the wall of die. From ambient temperature to 700 °C, it took 5 min to heat the sample. Then the temperature was increased up to needed temperature with a heating rate of 100 °C/min. The annealing temperature was selected as 1600 °C and the holding time was 5 min. During sintering, the uniaxial pressure was increased to 30 MPa before 1000 °C. After finishing the procedure, the sample was cooled down to ambient temperature with the cooling rate of furnace. For comparison, the sample sintered at 1800 °C was also prepared using the similar process.

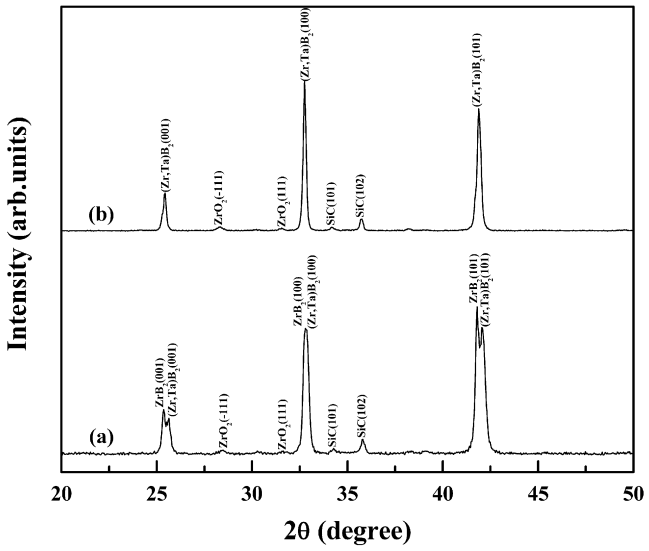

Fig. 1. X-ray diffraction (XRD) patterns of synthesized ZrB_2–SiC composites with $TaSi_2$ additive sintered at (a) 1600 °C and (b) 1800 °C.

The contaminations on the surface of samples were removed by a running diamond grinding wheel. All the samples were ground and polished down to 1.0 μm diamond grits. Phase compositions in the samples were examined by an X-ray diffraction (XRD) analyzer (JDX-3500, JEOL Ltd., Japan) with Cu Kα radiation. The polished surface of samples were examined by a scanning electron microscope (SEM) (JSM-7100F, JEOL Ltd., Japan) equipped with an energy dispersive spectroscopy (EDS) system. The surface morphologies and element distribution maps were obtained. Here, L3 mode was used to distinguish Ta and Si elements during EDS analysis. Thin specimens for transmission electron microscope (TEM) investigation were prepared by mechanically grinding down to a thickness of about 100 μm firstly. Then the disk samples with a diameter of 3 mm were cut off using an ultrasonic cutter (Gatan 601, Gatan Inc., CA) with SiC powder as the media. After that, the disks were dimpled to a thickness of ~20 μm in the center using a dimple grinder (Gatan 656, Gatan Inc., CA). For further thinning, Ar^+-ion beam at an accelerating voltage of 4 kV was used to make a hole in the center of samples with an angle of 3–7° in a Precision Ion Polishing System (PIPS™) (Gatan 691, Gatan Inc., CA). The microstructure was investigated by a TEM Apparatus (JEM-2100F, JEOL Ltd., Japan) operated at 200 kV. The high resolution atom images were obtained. Additionally, the scanning transmission electron microscope (STEM) was used to observe the dislocations in the boride grains. The TEM atom images were treated for Fast Fourier Transform (FFT) by a digital micrograph software (DM, Gatan Inc., CA).

3. Results and discussion

Fig. 1 shows the XRD patterns of synthesized ZrB_2–SiC composites with $TaSi_2$ additive sintered at 1600 and 1800 °C. Obviously, when the sample was sintered at 1600 °C, (Zr,Ta)B_2 solid solution appeared. The diffraction peaks of (Zr,Ta)B_2 deflect to higher angles in comparison with those of ZrB_2

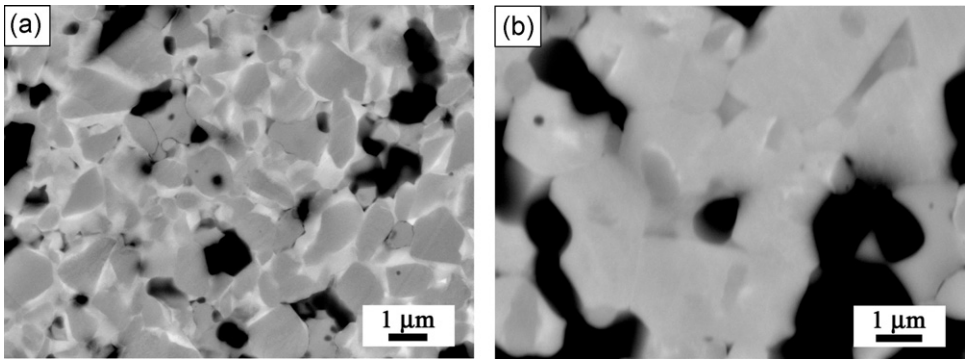

Fig. 2. Scanning electron microscope (SEM) images of polished surface of synthesized ZrB_2–SiC composites with $TaSi_2$ additive sintered at (a) 1600 °C and (b) 1800 °C.

(Fig. 1(a)). It is known that the atom radius of Ta (0.146 nm) is smaller than that of Zr (0.162 nm), which indicates that the solid solution of Ta atoms into ZrB_2 grains causes the crystal cell contraction reflecting the decrease of crystal parameters.[16–18] The Ta atoms come from the decomposition of $TaSi_2$. Because that there are no diffraction peaks of $TaSi_2$ existing in the spectra, it is considered that all of the $TaSi_2$ in the composite have decomposed and probably all the Ta atoms have entered the ZrB_2 grains to form solid solution. The decomposed Si atoms possibly evaporated at high temperature during sintering. Also, there was another possibility that silicon reacted with carbon to form silicon carbide owing to the carbon atmosphere in the graphite die. When increasing the sintering temperature up to 1800 °C, the diffraction peaks of ZrB_2 disappear (Fig. 1(b)), which is probably attributed to the homogeneous diffusion of Ta atoms in the ZrB_2 grains. As a result, the composite consists of solid solution $(Zr,Ta)B_2$ and SiC. In addition, a small amount of ZrO_2 was examined in the composites, which was probably introduced during the powder milling. Lee et al.[19] have determined that ZrO_2 existed in the milled ZrB_2 powder.

The solid solution and core–shell structure were proved by SEM investigation. Fig. 2 shows the polished surface of composites sintered at 1600 and 1800 °C. Obviously, it is observed that the gray-white shell distributes around the gray grains, i.e. the positions of ZrB_2 grain boundaries (Fig. 2(a)). SiC particles homogeneously distribute in the matrix and no agglomeration of SiC can be found. Also, no pores can be observed in the composite, which indicates the full densification. The mean particle sizes of boride and SiC are about 2 and 0.55 μm respectively, which means that the particles did not grow up during sintering. It seems that 1600 °C is a low sintering temperature which does not accelerate the grain growth. On the polished surface of composite prepared at 1800 °C, it is seen that there is no core–shell structure existing (Fig. 2(b)). The mean grain sizes of boride and SiC increase to about 4 and 1 μm respectively. It is concluded that the sintering process at higher temperature not only contributes to the Ta atom diffusion but also accelerates the grain growth. It can be imaged that the high concentration of Ta atoms in the shell structure supplies the potential to diffuse into the inner core.[20] The higher sintering temperature provides the drive force. Otani et al.[21] confirmed that ZrB_2 and TaB_2 could form the complete solid solution with any composition. It means that in the composite Ta atoms can diffuse homogeneously to obtain the uniform Ta atom concentration in the boride grains. Also, the grain growth is achieved by grain boundary atom diffusion at higher sintering temperature. Fig. 3 shows the element distribution of polished surface of sample sintered at 1600 °C. Owing to the close energy of Si Kα1 (1.74 keV) and Ta Mα1 (1.71 keV), it is difficult to distinguish the elements of Si and Ta at low energy level by EDS analysis, as reported before.[10] Here, L3 mode was adopted, which could clearly identify the Ta Lα1 (8.14 keV) and Ta Lβ1 (9.34 keV) peaks.[22] Corresponding to the SEM image, in which the black particle is SiC, gray region is ZrB_2, and gray-white region is $(Zr,Ta)B_2$, Zr, B, Si, and Ta element distributions are obviously seen in Figs. 3(b)–(e). Zr and B elements have the same distribution (green and red colors). Si element exists in the positions of SiC particles (brown color). Ta element lies in the positions of gray-white shell (blue color). That is, Ta element just exists in the grain boundaries of boride with the formation of $(Zr,Ta)B_2$. Based on the result that Mo element could decrease the grain boundary active energy and accelerate the atom diffusion process,[23] it is supposed that Ta element has the similar effect. Also, Ta atoms themselves participate in the diffusion process. When the sintering temperature was increased up to 1800 °C, the matrix of composite became homogeneous. Ta element has the same distribution with Zr and B elements (Fig. 4(b)–(e)), which indicates the complete and homogeneous solid solution of Ta atoms in ZrB_2 grains. This result is corresponding to the disappearance of core–shell structure.

Furthermore, the boundaries between boride grains, as well as between boride grains and SiC particles, were observed by TEM. Fig. 5 shows the bright field transmission electron microscope (TEM) image and high resolution atom image of two combining boride grains in the ZrB_2–SiC composite with $TaSi_2$ additive sintered at 1600 °C. It is seen that there is no amorphous phase existing at the grain boundary (Fig. 5(a) and (b)). Two boride grains have the coherent structure with the zone axes of [0 1 0]//[0 0 1], as shown in the inset of Fig. 5(b). It means that the solid solution of Ta atoms into ZrB_2 grains does not change the crystal structure orientation of close grains and just makes the grains "sewing" together by forming the coherent structure. Additionally, the grain boundaries between boride and SiC were

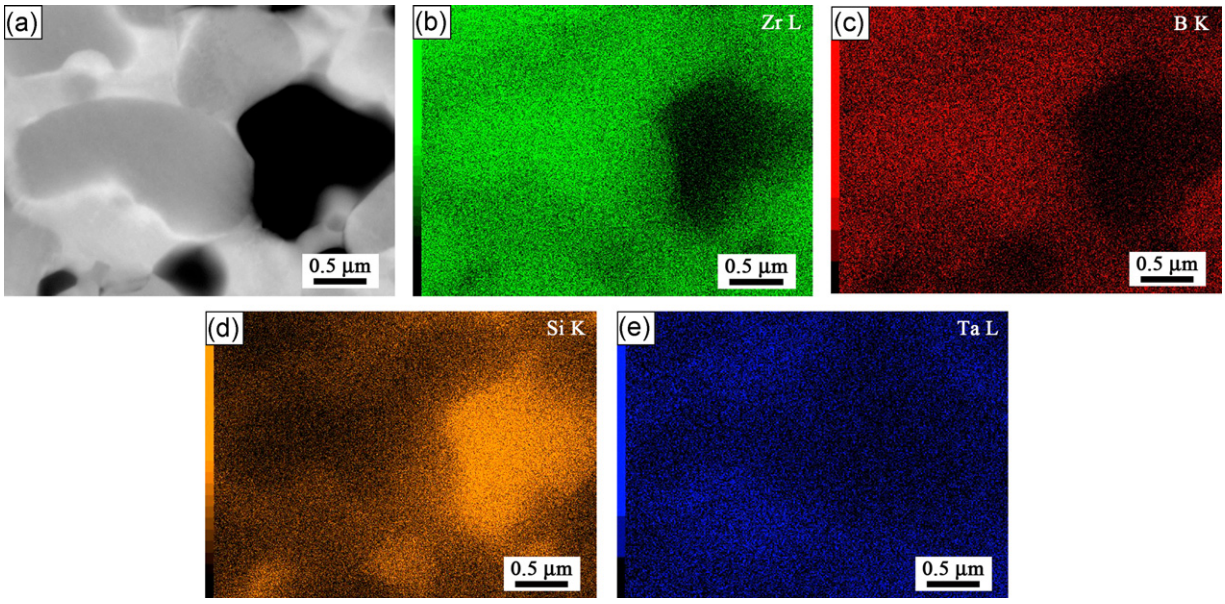

Fig. 3. (a) SEM micrograph of polished surface of ZrB_2–SiC composite with $TaSi_2$ additive sintered at 1600 °C, and the element distribution maps corresponding to (a): (b) Zr element, (c) B element, (d) Si element, and (e) Ta element.

also examined, as shown in Fig. 6. Fig. 6(a) shows the phase distribution of compositions in the composite. Except the phases of boride and SiC, ZrO_2 was examined corresponding to the XRD result. Lee et al.[24] determined that the fresh surface of ZrB_2 particles during milling was easily covered by oxides. In Fig. 6(b), amorphous phase is not observed at the grain boundary. Boride forms the coherent structure with SiC with the zone axes of [1 0 1]//[0 0 1]. It is confirmed that the silicon from the decomposition of $TaSi_2$ probably has completely evaporated and/or reacted with carbon at high temperature. It is concluded that for present case 10 vol.% $TaSi_2$ additive does not result in the silicon remnant in the composite after sintering.

The existence of dislocations in the boride grains indicates the effect of pressure on densification during spark plasma sintering. Mizuguchi et al.[25] found that the dislocations originated from the ZrB_2 grain boundaries and crossed the grains in the SPSed sample. Surely, the same phenomenon was observed by STEM, as shown in Fig. 7. Obviously, in the boride grain, the high density dislocations emanate and propagate from the grain boundary. Several parallel dislocation walls go through the grain.

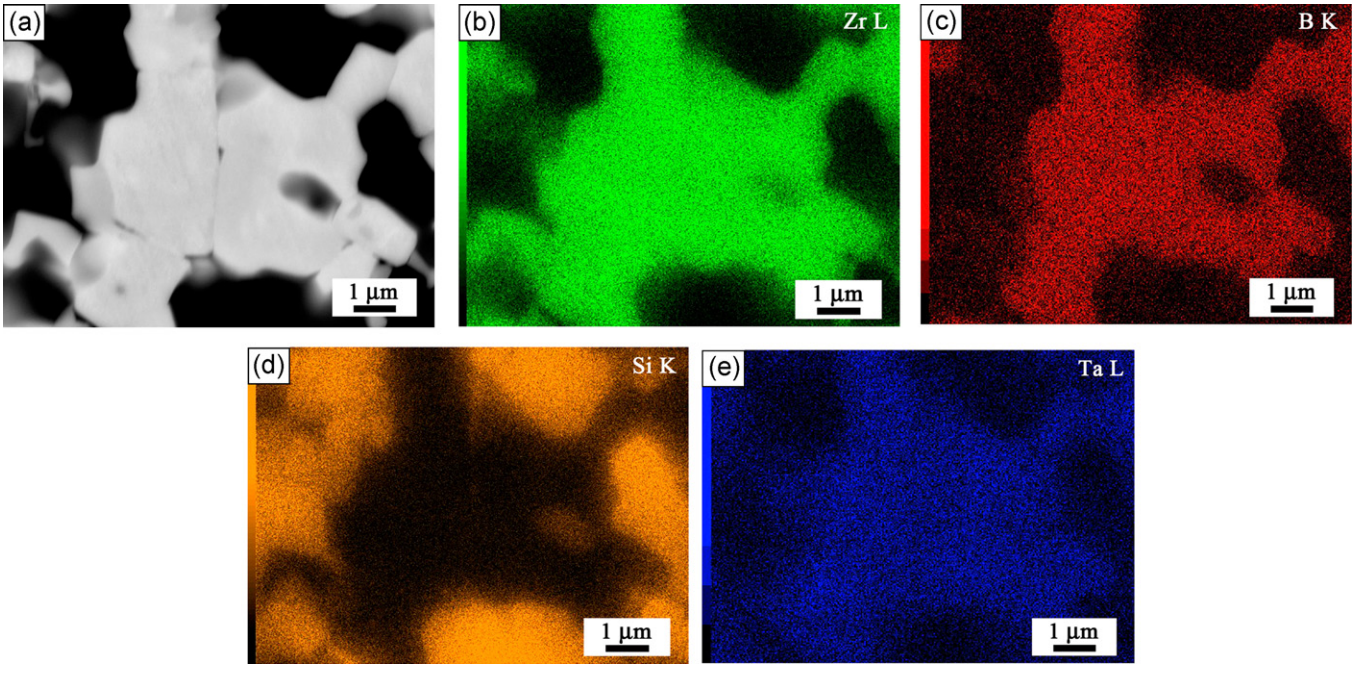

Fig. 4. (a) SEM micrograph of polished surface of ZrB_2–SiC composite with $TaSi_2$ additive sintered at 1800 °C, and the element distribution maps corresponding to (a): (b) Zr element, (c) B element, (d) Si element, and (e) Ta element.

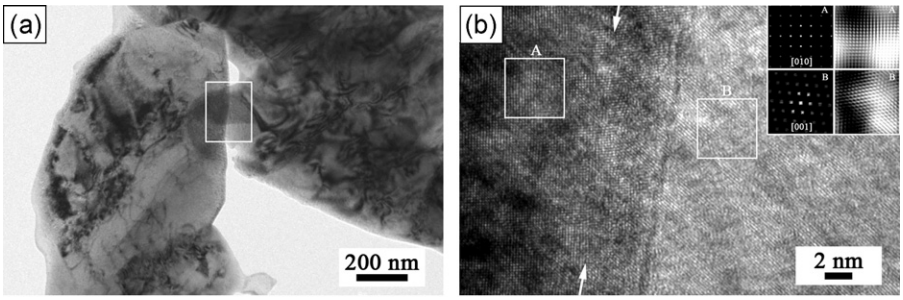

Fig. 5. (a) Bright field transmission electron microscope (TEM) image of ZrB_2–SiC composite with $TaSi_2$ additive sintered at 1600 °C, which shows two boride grains. (b) High resolution atom image of the assigned grain boundary region in (a). Inset images in (b) are the diffraction patterns and atom arrangement images treated by Fast Fourier Transform (FFT) at the A and B regions. The arrows indicate the grain boundary.

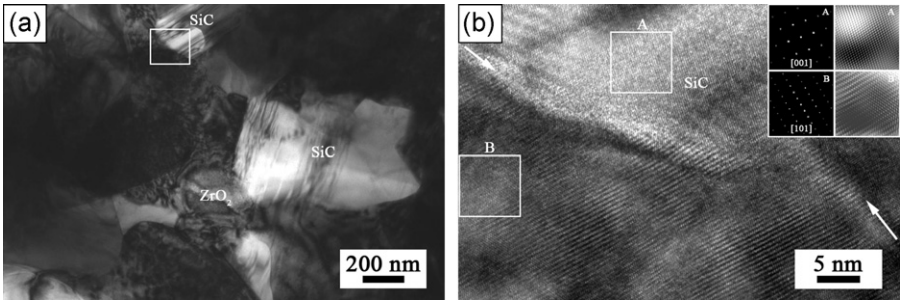

Fig. 6. (a) Bright field TEM image of ZrB_2–SiC composite with $TaSi_2$ additive sintered at 1600 °C. (b) High resolution atom image of the assigned boride and SiC grain boundary region in (a). Inset images in (b) are the diffraction patterns and atom arrangement images treated by FFT at the A and B regions. The arrows indicate the grain boundary.

In previous investigation of SPSed ZrB_2–ZrC composite, Kim and Shim[26] observed the well-ordered dislocation arrays with large area in the ZrB_2 grain. It was considered that the high and localized stresses induced by the sharp thermal gradient during the SPS process might cause the plastic deformation of ZrB_2 grain for forming dislocation structure. It means that during the sintering the pressure contributes to the densification by compacting the grains and causing the plastic deformation.

In addition, the microstructure of composite prepared at 1800 °C was also investigated by TEM for comparison. Fig. 8 shows the bright field TEM image of sample and the atom images of the grain boundaries between $(Zr,Ta)B_2$ and SiC and between two $(Zr,Ta)B_2$ grains. It is seen that the amorphous phase is still absent at the grain boundaries, the grain boundaries are very clear and only the coherent structures can be found. This result indicates that there is no amorphous phase existing in the prepared composite. By combining the investigation results, it is expected that it is probably a good way to densify ZrB_2 at low temperature using the solid solution. Because many other elements such as Ti, Nb, and Hf can form the complete solid solutions with ZrB_2,[21] it is promising to use the corresponding silicides $TiSi_2$ (melting point, 1480 °C), $NbSi_2$ (melting point, 1940 °C), and $HfSi_2$ (melting point, 1543 °C) as the sintering additives.

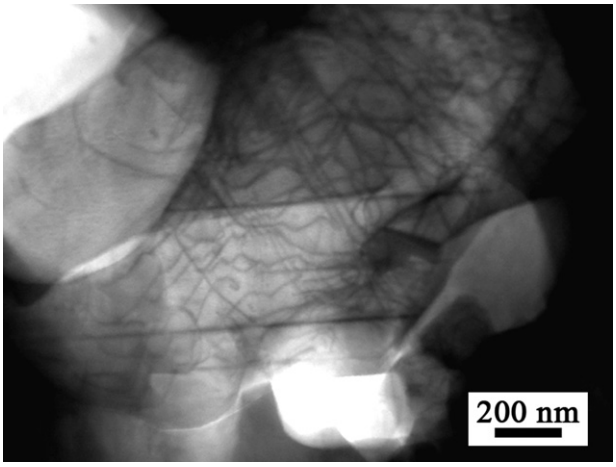

Fig. 7. Scanning transmission electron microscope (STEM) image of ZrB_2–SiC composite with $TaSi_2$ additive sintered at 1600 °C, showing the obvious dislocations in the boride grain.

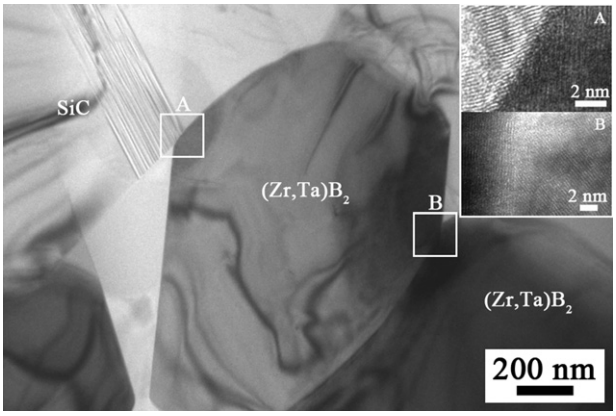

Fig. 8. Bright field TEM image of ZrB_2–SiC composite with $TaSi_2$ additive sintered at 1800 °C. Inset figures show the grain boundaries between $(Zr,Ta)B_2$ and SiC and between two $(Zr,Ta)B_2$ grains at the A and B regions.

4. Conclusions

Dense ZrB_2–SiC composite was fabricated at the low temperature of 1600 °C by SPS with 10 vol.% $TaSi_2$ additive. The microstructure observation showed that core–shell structure existed in the sample in which the core was ZrB_2 and the shell was the solid solution of (Zr,Ta)B_2. The solid solution of Ta atoms into ZrB_2 grains decreased the boride grain boundary active energy, which contributed to the formation of coherent structure of boride grain boundaries. Additionally, the existence of dislocations in the boride grains indicated that the pressure during spark plasma sintering also imposed the important effect on the densification of composite. Additionally, when the composite was prepared at the higher temperature of 1800 °C, Ta atoms distributed homogeneously in the boride grains, which resulted in the disappearance of core–shell structure. The grain boundaries investigation between (Zr,Ta)B_2 grains and between boride and SiC showed that the grain boundaries were still clear without the amorphous phase existing.

Acknowledgements

This work was partially supported by Grant-in-Aid B (No. 20350099) for Scientific Research from the JSPS of Japan and also World Premier International Research Center (WPI) Initiative, MEXT, Japan.

References

1. Mroz C. Zirconium diboride. *Am Ceram Soc Bull* 1994;**73**:141–2.
2. Chamberlain AL, Fahrenholtz WG, Hilmas GE, Ellerby DT. High strength zirconium diboride-based ceramics. *J Am Ceram Soc* 2004;**87**: 1170–2.
3. Ni DW, Zhang GJ, Kan YM, Sakka Y. Highly textured ZrB_2-based ultrahigh temperature ceramics via strong magnetic field alignment. *Scr Mater* 2009;**60**:615–8.
4. Bull J, White MJ, Kaufman L. Ablation resistant zirconium and hafnium ceramics. United States Patent 5750450; 12 May 1998.
5. Monteverde F, Savino R. Stability of ultra-high-temperature ZrB_2–SiC ceramics under simulated atmospheric re-entry conditions. *J Eur Ceram Soc* 2007;**27**:4797–805.
6. Guo SQ. Densification of ZrB_2-based composites and their mechanical and physical properties: a review. *J Eur Ceram Soc* 2009;**29**: 995–1011.
7. Guo SQ, Kagawa Y, Nishimura T. Mechanical behavior of two-step hot-pressed ZrB_2-based composites with $ZrSi_2$. *J Eur Ceram Soc* 2009;**29**:787–94.
8. Guo SQ, Nishimura T, Mizuguchi T, Kagawa Y. Mechanical properties of hot-pressed ZrB_2–$MoSi_2$–SiC composites. *J Eur Ceram Soc* 2008;**28**:1891–8.
9. Sciti D, Silvestroni L, Celotti G, Melandri C, Guicciardi S. Sintering and mechanical properties of ZrB_2–$TaSi_2$ and HfB_2–$TaSi_2$ ceramic composites. *J Am Ceram Soc* 2008;**91**:3285–91.
10. Talmy IG, Zaykoski JA, Opeka MM, Smith AH. Properties of ceramics in the system ZrB_2–Ta_5Si_3. *J Mater Res* 2006;**21**:2593–9.
11. Hu CF, Sakka Y, Tanaka H, Nishimura T, Guo SQ, Grasso S. Microstructure and properties of ZrB_2–SiC composites prepared by spark plasma sintering using $TaSi_2$ as sintering additive. *J Eur Ceram Soc* 2010;**30**:2625–31.
12. Mizuguchi T, Guo SQ, Kagawa Y. Transmission electron microscopy characterization of hot-pressed ZrB_2 with $MoSi_2$ additive. *J Am Ceram Soc* 2009;**92**:1145–8.
13. Maizza G, Grasso S, Sakka Y, Noda T, Ohashi S. Relation between microstructure, properties and spark plasma sintering (SPS) parameters of pure ultrafine WC powder. *Sci Technol Adv Mater* 2007;**8**:644–54.
14. Grasso S, Sakka Y, Maizza G. Electric current activated/assisted sintering (ECAS): a review of patents 1906–2008. *Sci Technol Adv Mater* 2009;**10**:053001.
15. Orrù R, Licheri R, Locci AM, Cincotti A, Cao G. Consolidation/synthesis of materials by electric current activated/assisted sintering. *Mater Sci Eng Rep* 2009;**63**:127–287.
16. Talmy IG, Zaykoski JA, Opeka MM. High-temperature chemistry and oxidation of ZrB_2 ceramics containing SiC, Si_3N_4, Ta_5Si_3, and $TaSi_2$. *J Am Ceram Soc* 2008;**91**:2250–7.
17. Saida J, Sanada T, Sato S, Imafuku M, Li CF, Inoue A. Nano quasicrystal formation and local atomic structure in Zr–Pd and Zr–Pt binary metallic glasses. *Z Kristallogr* 2008;**223**:726–30.
18. Pérez RA, Dyment F, Bermúdez GG, Abriola D, Behar M. Diffusion of Ta in α-Ti. *Appl Phys A* 2003;**76**:247–50.
19. Lee SH, Sakka Y, Kagawa Y. Dispersion behavior of ZrB_2 powder in aqueous solution. *J Am Ceram Soc* 2007;**90**:3455–9.
20. Wiesenberger H, Lengauer W, Ettmayer P. Reactive diffusion and phase equilibria in the V–C, Nb–C, Ta–C and Ta–N systems. *Acta Mater* 1998;**46**:651–66.
21. Otani S, Aizawa T, Kieda N. Solid solution ranges of zirconium diboride with other refractory diborides: HfB_2, TiB_2, TaB_2, NbB_2, VB_2 and CrB_2. *J Alloys Compd* 2009;**475**:273–5.
22. Peng F, Berta Y, Speyer RF. Effect of SiC, TaB_2 and $TaSi_2$ additives on the isothermal oxidation resistance of fully dense zirconium diboride. *J Mater Res* 2009;**24**:1855–67.
23. Kislui PS, Kuzenkova MA. Regularities of sintering zirconium diboride–molybdenum alloys. *Sov Powder Metall Met Ceram* 1966;**5**:360–5.
24. Lee SH, Sakka Y, Kagawa Y. Corrosion of ZrB_2 powder during wet processing—analysis and control. *J Am Ceram Soc* 2008;**91**:1715–7.
25. Mizuguchi T, Guo SQ, Kagawa Y. Transmission electron microscopy characterization of spark plasma sintered ZrB_2 ceramic. *Ceram Int* 2010;**36**:943–6.
26. Kim KH, Shim KB. The effect of lanthanum on the fabrication of ZrB_2–ZrC composites by spark plasma sintering. *Mater Charact* 2003;**50**:31–7.